ELSEVIER

Engineering Structures 22 (2000) 1189–1194

ENGINEERING STRUCTURES

www.elsevier.com/locate/engstruct

Finite-element strength and stability analysis and experimental studies of a submarine-launched missile's composite dome

Jinsong Huang *, Guangwu Zeng

Department of Naval Architecture and Ocean Engineering, HUST, Wuhan, 430074, People's Republic of China

Received 3 August 1998; received in revised form 11 January 1999; accepted 30 March 1999

Abstract

The paper presents a finite element model for strength analysis of a submarine-launched missile's composite dome under axial tension and internal pressure. Characteristics of stress distribution and locations and loads of failure are determined according to the model. Another finite element model is developed to calculate stability of the dome under axial compression, external pressure and the combination of axial compression and external pressure. Experiments are completed for studying the strength of the dome under axial compression and internal pressure and the stability of the dome under the combination of axial compression and external pressure.

Keywords: Structural strength; Stability; Experimental study; Dome

1. Structural strength analysis

1.1. Construction of the finite-element model

The structural contour of the fairing studied in this paper is a rotational thin-shell, which consists of a long thin-shell structure and a short cylindrical shell structure (transitional part). The main body of the structure is made of seven-ply laminated woods. The longitudinal veined layer of the wood alternates with the transverse veined layer of the wood from the outer surface to the inner surface of the shell. The ends of the shell are made of aluminum, as shown in Fig. 1. This kind of structural model has been applied to many actual engineering structures [1–3]. Although the structure is axial symmetrical, the whole part of the structure is included in the finite-element model due to the asymmetry of openings and auxiliary structures. The aluminum at the ends of the structure are modeled with two layers of meshes. Laminated woods in the middle of the structure are modeled with fifteen layers of meshes. The mesh is coarse in the middle and becomes finer when it reaches the ends. A bolt hole is arranged every ten degrees of angle

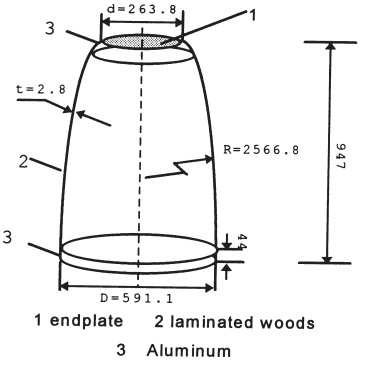

Fig. 1. Contour of the fairing (unit: mm).

and then thirty-six layers of meshes are modeled in circumference. The model contains 720 nodes and 684 elements (540 elements in layers of wood and 144 elements in layer of aluminum), as shown in Fig. 2. Composite thin shell/plate element (for laminated woods) and thin shell/plate element (for aluminum) are used. Both kinds of element are based on the Kirchhoff Love shell theory.

1.2. Loading conditions and boundary conditions

In loading condition of lift (as shown in Fig. 3), an axial tension is applied to the structure. The endplate is

* Corresponding author.
E-mail address: jishuang@wuhee.edu.cn (J. Huang).

PII: S0141-0296(99)00040-1

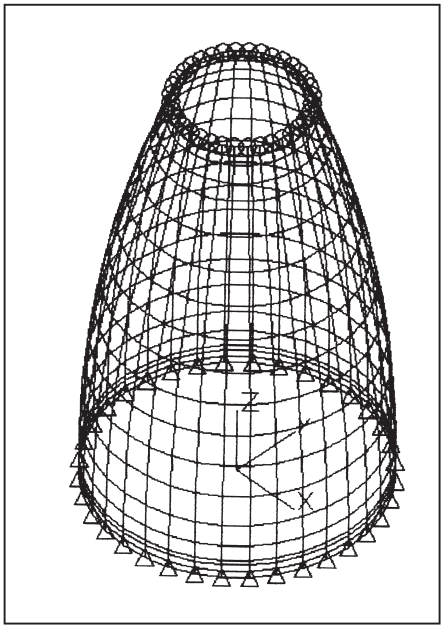

Fig. 2. Distribution of finite-element meshes.

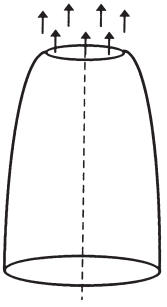

Fig. 3. Load case of axial compression.

considered as a rigid plate since the stiffness of the endplate is much larger than the stiffness of the thin-shell structure. The axial tension is then uniformly distributed to boundary nodes at the top of the fairing. (The force is transmitted by the bolt at the same place in the actual condition.)

In loading condition of internal pressure (as shown in Fig. 4), the sealed fairing is subjected to the uniformly distributed internal pressure. The axial tension due to the internal pressure on the endplate is uniformly distributed on boundary nodes at the top of the fairing. In addition, uniformly distributed internal pressure is applied to each of the elements.

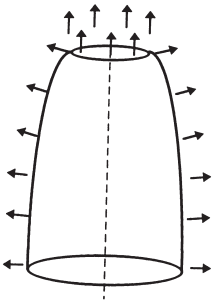

Fig. 4. Load case of external pressure.

Boundary conditions are shown in Fig. 2, where △ represents fix-supported (all the degrees of freedom are restrained), ○ represents roller-supported (all the degrees of freedom are restrained except for the vertical degree (direction *z*) of freedom).

The joint of wood and aluminum laminated structure is not uniformly edged. However, the element distribution is modeled to the whole laminated plate and the variance of the length of each layer is not considered. So the mean length of those layers is used in the calculation.

1.3. Material properties

Material properties of wood are determined by relative material testing and from the handbook of the material.

Material properties of wood:

Principal Young's modulus E_{Ll}:	10.416 (GPa)
Longitudinal veined tensile strength F_{Ll}:	104.00 (MPa)
Minor Young's modulus E_{Tl}:	1.644 (GPa)
Longitudinal veined compressive strength F_{Lc}:	69.51 (MPa)
Major Poisson's ratio V_{LT}:	0.343
Transverse veined tensile strength F_{Tl}:	24.77 (MPa)
Shearing modulus E_{LT}:	1.6 (GPa)
Transverse veined compressive strength F_{Tc}:	17.91 (MPa)
Shearing strength F_{LT}:	8.5 (MPa)

According to references, the material properties of Aluminum are given in the following.

Young's modulus	71 GPa
Shearing strength	27 GPa
Poisson's ratio	0.32
Tensile ultimate strength	350 MPa

1.4. Failure criterion

The failure criterion used in this paper is the Tsai-Wu criterion of orthotropic material subjected to the plane stress.

$$K_1\sigma_1+K_2\sigma_2+K_{11}\sigma_1^2+K_{22}\sigma_2^2+K_{66}\tau_{12}^2+K_{12}\sigma_1\sigma_2=1$$

Where σ_1, σ_2, τ_{12} are major principal stress, minor principal stress and shearing stress, respectively. The following parameters may be obtained from basic parameters of material testing:

$$K_1=1/F_{LI}-1/F_{LC}\quad K_2=1/F_{TI}-1/F_{TC}\quad K_{11}=1/(F_{LI}\cdot F_{LC})$$

$$K_{22}=1/(F_{TI}\cdot F_{TC})\quad K_{66}=1/F_{LT}^2$$

Table 1
Locations and loads of failure

Loading condition	Predicted values of failure	Location of failure
Lift	209.1 kN	The seventh layer of wood at the joint of wood and aluminum in the smaller end (longitudinal veined wood)
Internal pressure	0.545 MPa	The first layer of wood at the joint of wood and aluminum in the larger end (longitudinal veined wood)

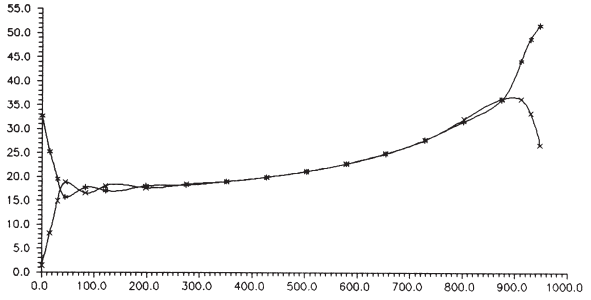

Fig. 5. Axial stress distribution under loading condition of fit.

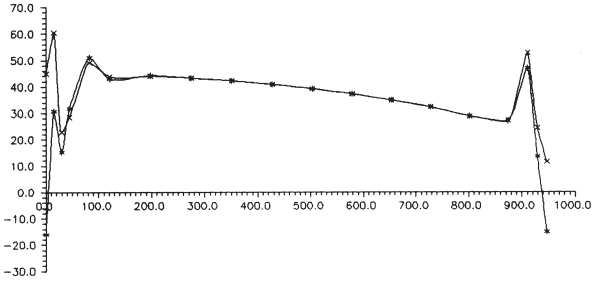

Fig. 7. Circumferential stress distribution under loading condition of internal pressure.

The parameter K_{12} is determined by the bitensile (bicompressive) testing. In the program, we use the following approximate calculation

$$K_{12} = -\sqrt{K_{11} \cdot K_{22}}$$

1.5. Results and analysis

According to the failure criterion, predicted locations and loads of failure are shown in Table 1. Axial distribution of mean stresses in different loading conditions are shown in Figs. 5–7 (×=Stress of the inner surface, *=stress of the outer surface). Characteristics of stress distributions of the structure can be seen from the figures: High stress zone is shown in the ends of the fairing with fluctuating variation. The maximum stress in this area has reached the "critical stress". However, the structure still has some bearing capacity for high loading. The fact provides some guidance for the "end-stiffened" optimum design.

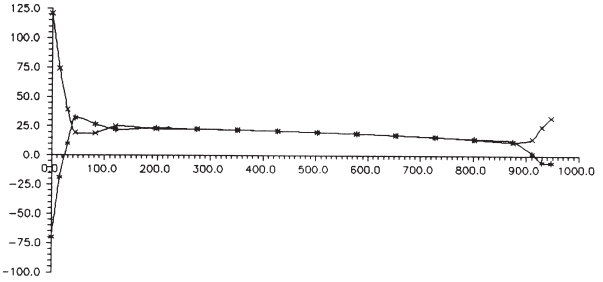

Fig. 6. Axial stress distribution under loading condition of internal pressure.

According to the assumptions in material mechanics, the in-plane strain of each element in different layers is the same. So the layer which has a large Young's modulus in the direction of loading has to bear a relatively large load and the failure is mainly determined by the ratio of the Young's modulus and the limit of strength in the direction of loading. A larger ratio means an earlier failure. The ratio of the Young's modulus and the limit of strength of material studied in this paper in the longitudinal direction is larger than that in the transverse direction. So all failures occur at longitudinal layers in the above loading conditions.

2. Calculation of stability

2.1. Material properties

The stability of the laminated structure is mainly related to the whole stiffness of the material. So the orthotropic model is used to simplify the calculation. Orthotropic thin shell/plate element (for laminated woods) and thin shell/plate element (for aluminum) are used. Both kinds of element are based on the Kirchhoff Love shell theory.

Material properties of the laminated woods are determined by relative material testing and the handbook of the material.

Principal Young's modulus:	6.656 (GPa)
Minor Young's modulus:	5.403 (GPa)

Major Poisson's ratio:	0.154
Shearing modulus:	1.6 (GPa)

2.2. Calculation of stability

The module of buckling analysis of shell/plate structure in the finite-element analysis program is used to calculate the fairing (including the aluminum in the ends). The laminated aluminum plate at each end is modeled with a layer of meshes along the generating line. Laminated woods in the middle of the structure are modeled with fifteen layers of meshes. The mesh is coarse in the middle and becomes finer when it reaches the ends. 24 layers of meshes are modeled in circumference. The model contains 432 nodes and 408 elements. One problem should be specified here: The value of the critical load will become lower if the mesh becomes finer in the calculation. The error of calculation due to mesh size is less than 3% finally. The boundary condition is the same as that in the strength calculation. In the load case of axial compression the direction of force is opposite to that of the load case of lift. In the load case of external pressure the direction of force is opposite to that of the load case of internal pressure. The simplification of external loads is similar to that in the strength calculation. Results of the calculation are shown in Table 2.

3. Experimental studies

3.1. Experimental set-up

The experimental equipment shown in Fig. 8 is used for convenience of loading. The top of the model is fastened to a connector and the seam is filled with plasticine. The outer seam is sealed with 703 silica gel. The bottom of the model is connected with the transitional plate by a screw connection. 703 silica gel is filled around the screw. A ring rubber washer is placed into the ring groove in the joint of the transitional plate and the stern transom plate. The nut under the stern transom plate is tightly welded to prevent sinking and to change models conveniently. The axial compressive load is simulated by a loading to the lift bolt through a hydraulic jack. A pressure gage is placed at the top of the jack. Centering of the system is required before the experiment to ensure the axial symmetry of loading. External pressure is simulated by vacuuming the inside of the fairing. The vacuum pump is directly connected with the feed-water pipeline. A control valve is used to adjust the ratio of vacuum.

Table 2
Results of calculation

Loading condition	Orthotropic finite-element
Axial compression	287.8 kN
External pressure	0.0999 MPa
Combination of axial compression and external pressure	115.19 kN/0.11519 MPa

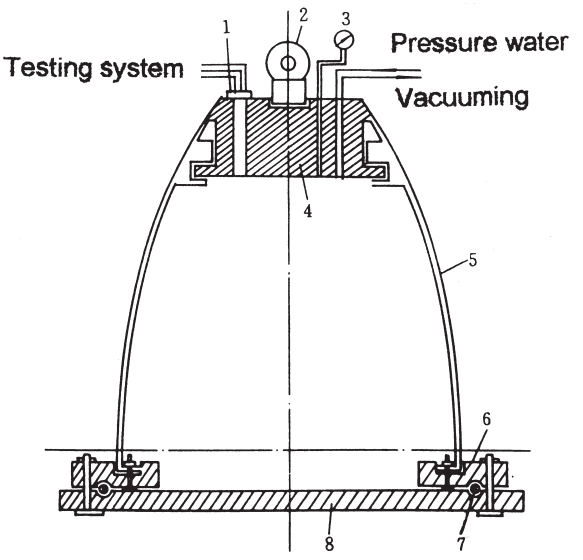

Fig. 8. Experimental set-up. 1, Waterproof joint; 2, lift bolt; 3, pressure gage; 4, connector; 5, model; 6, transitional plate; 7, rubber washer; 8, stern transom plate.

3.2. Experiment of failure under axial compression

The structure is loaded by an increment of 4.9 kN. The rate of loading is reduced when the load reaches 39.2 kN. When the load reaches 53.9 kN, three-fourths part of the joint of wood and aluminum in circumference is fractured at the smaller end of the model. Fig. 9 shows the failure of the model under load of axial compression.

Fig. 9. Failure under axial compression.

Materials of wood and aluminum are separated. The remaining parts of the model are intact. Most aluminum foils are peeled off completely at the fracture of the inner layer. The estimated shearing stress between layers is 1.4 MPa in this case. It shows that the adhesive strength is not large enough and the fracture belongs to the failure of local strength. The load of failure under lift loading conditions is nearly 53.9 kN in this case. The value is far lower than the predicted load of failure.

3.3. Experiment of failure under internal pressure

The structure is loaded by an increment of 0.05 MPa. The rate of loading is reduced when the load reaches 0.3 MPa. The model is split along the longitudinal direction when the load reaches 0.47 MPa. The first fracture happens at the joint of wood and aluminum at the large end of the model. An obvious initial imperfection is found near to that location. The model is teared at the joint of wood and Aluminum along the circumference direction at first. It is then split along the longitudinal direction and the crevice extends to the joint of wood and aluminum at the smaller end. Fig. 10 shows the failure of the model under the load of internal pressure.

3.4. Experiment of failure under a combination of axial compression and external pressure

The structure is loaded by increments of 4.9 kN and 0.005 MPa. The axial compression keeps constant after the load reaches 39.2 kN/0.04 MPa. The model is continuously vacuumed and loaded by an increment of 0.005 MPa. The reading of the pressure gage shows that the axial compression becomes lower in the period of vacuuming. It suggests that the whole axial deformation under the external pressure is a shrinkage deformation. After the external pressure reaches 0.06 MPa, the rate of vacuuming is obviously slowed down due to the vaporization of the residual water in the experiment of internal pressure. It is benefit for adjusting the rate of loading. The value of strain is measured when the load reaches 0.08 MPa. The external pressure is constant in a relatively long time period. When the load reaches 0.081 MPa, the model is fractured suddenly with a loud noise. Middle parts of the model collapse and the cross-section of the fracture is uniform in general. Layer separations do not occur in most locations of fracture. No large deformation happens before the fracture of the model. The zone near the ends and the parts of the joint remain, which shows the failure is a typical over-all buckling of structure. Fig. 11 shows the failure of the model in this case.

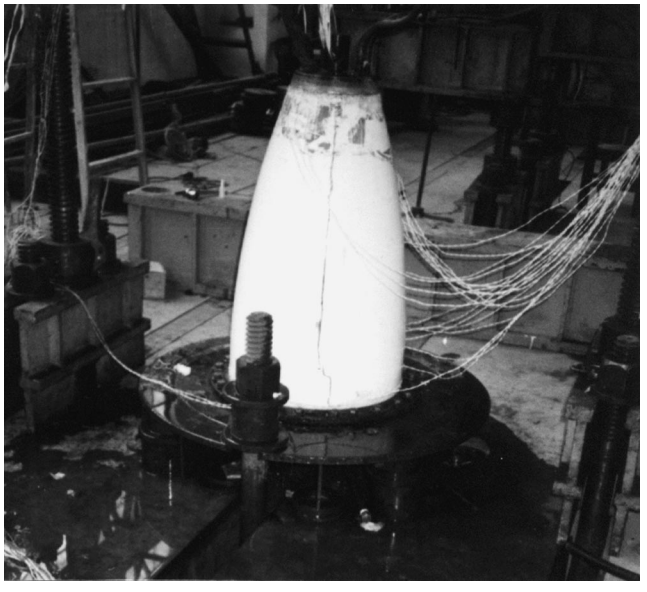

Fig. 10. Failure under internal pressure.

4. Conclusions

Characteristics of stress distributions of the structure are that a high stress zone is shown at the ends of the fairing with fluctuating variation. The maximum stress in this area has reached the “critical stress”. However, the structure still has some bearing capacity for high loading. The fact provides some guidance for the “end-stiffened” optimum design. It can reduce the weight of the submarine-launched missile and reinforce its attack abilities.

The experiment shows that the failure of the structure under axial compression is caused by the failure of local strength. The results show that the strength of the structure under axial compression is mainly related to the cohesion strength between wood and aluminum. This shows that to seek a new bond that has a high cohesion strength between wood and aluminum is very important. The model tears at the bottom joint of wood and alumi-

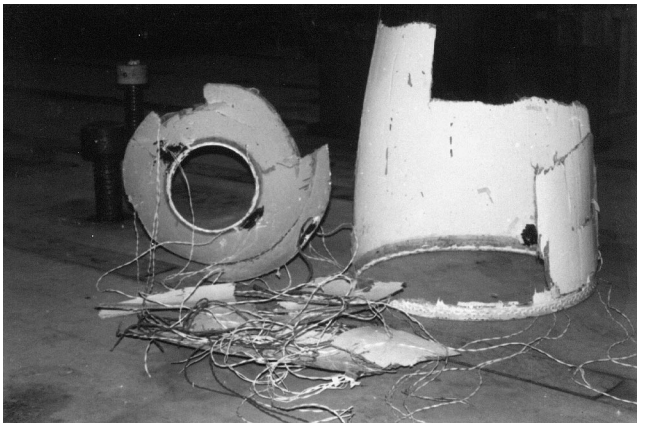

Fig. 11. Failure under combination of axial compression and external pressure.

num along the circumference direction at first in the load case of internal pressure. It shows that in this case the imperfection in the bottom area of the structure is very sensitive because of the high stress level in this area. Experiments also show that the failure of the structure under a combination of axial compression and external pressure is a typical over-all buckling.

References

[1] Xie Z., The nose of the "trident" I-type missile, Overseas Missile Technology, 1980:6.
[2] The A_3 Polaris Nose Fairing—A Structural composite of wood and aluminum, 8th International SAMPE Symposium, 1963.
[3] Wang Z. Mechanics and structural mechanics of composite materials. China Mechanical Industry Press, 1991.